Bioactive Calcium Phosphate Coatings on Metallic Implants

M. B. Sedelnikova[1,a)], E. G. Komarova[1,b)], Yu. P. Sharkeev[1,2,c)],
T. V. Tolkacheva[1,d)], I. A. Khlusov[2,3,4,e)], and V. V. Sheikin[3,f)]

[1] *Institute of Strength Physics and Materials Science SB RAS, Tomsk, 634055 Russia*
[2] *National Research Tomsk Polytechnic University, Tomsk, 634050 Russia*
[3] *Siberian State Medical University, Tomsk, 634050 Russia*
[4] *Immanuel Kant Baltic Federal University, Kaliningrad, 236041 Russia*

a) Corresponding author: smasha5@yandex.ru
b) katerina@ispms.tsc.ru
c) sharkeev@ispms.tsc.ru
d) tolkacheva@ispms.tsc.ru
e) khlusov63@mail.ru
f) tsws@ssmu.ru

Abstract. Biocomposites based on bioinert metals or alloys and bioactive calcium phosphate coatings are a promising tendency of the new-generation implants development. In recent years, the approach of regenerative medicine based on the use of biodegradable biomaterials has been priority direction. Such materials are capable of initiating the bone tissue regeneration and replaced by the newly formed bone. The microarc oxidation (MAO) method allows obtaining the bioactive coatings with a porous structure, special functional properties, and modified by the essential elements. During the last decade, the investigations in the field of the nanostructured biocomposites based on bioinert Ti, Zr, Nb and their alloys with a calcium phosphate coatings deposited by the MAO method have been studied in the Institute of Strength Physics and Materials Science SB RAS, Tomsk. In this article the possibility to produce the bioactive coatings with high antibacterial and osseoconductive properties due to the introduction in the coatings of Zn, Cu, Ag, La, Si elements and wollastonite $CaSiO_3$ was shown. The high hydrophilic and bioresorbed coatings stimulate the processes of osseointegration of the implant into the bone tissue. A promising direction in the field of the medical material science is a development of the metallic implants with good biomechanical compatibility to the bone, such as Ti-Nb alloys with a low elastic modulus that can be classified as biomaterials of the second generation. Zr and its alloys are promising materials for the dentistry and orthopedic surgery due to their high strength and corrosion resistance. Biodegradable Mg alloys are biomaterials of third generation. Such materials can dissolve with a certain speed in human body and excreted from the body thereby excluding the need for reoperation. This article presents the analysis of the study results of bioactive MAO coatings on Ti, Ti-Nb, Zr-Nb and Mg alloys and their promising medical application.

1. INTRODUCTION

In recent years, the approach of regenerative medicine based on the use of biodegradable biomaterials has been priority direction. Such materials can initiate the bone tissue regeneration and be replaced by the newly formed bone. Biocomposites based on bioinert metals or alloys and bioactive calcium phosphate (CaP) coatings are a promising tendency of the new-generation implants development [1].

Traditional biomedical metal materials such as stainless steels (316L), titanium alloys (e.g., Ti6Al4V) and cobalt–chromium–based alloys have been widely used as orthopedic implants. Since these metal implants should be removed after the first operation, another surgical intervention is necessary [2]. Ti and its alloys are widely used as both orthopedic and dental implants due to their excellent mechanical properties, high corrosion resistance, and biocompatibility [3]. But elastic modulus of Ti and its alloys ranges from 100 to 120 GPa that is significantly higher than the elastic modulus of bone tissue varied from 15 to 55 GPa. The low elastic modulus of the implant material

allows providing the uniform distribution of strains and stresses in the «bone-implant» system. In this case, the risk of the bone destruction decreases [4]. Therefore, a promising direction of the medical material sciences is the use of bioinert β-titanium alloys with a low elastic modulus such as Ti-Nb alloys. The doping of titanium with niobium in a concentration of 40–55 wt % allows decreasing in the elastic modulus of the alloy to 55–60 GPa that is comparable with that of the bone tissue [5].

Zr and its alloys are promising materials for the dental implants and load-bearing prostheses due to their high strength and corrosion resistance [6]. Unfortunately, Zr alloys as well as other bioinert metals and alloys show low binding between implant and bone tissue in early stages of osseointegration. This problem can be solved by the surface treatment and deposition of bioactive coatings [7, 8].

Mg and its alloys are biodegradable in human body fluids, and the corrosion product of Mg-based alloys is likely to be physiologically beneficial [9, 10]. Moreover the mechanical properties of Mg alloys are similar to those of natural bone [2]. In recent years, Mg alloys are being reconsidered for use as biodegradable implant materials for bone implants as well as for cardiovascular stents [10].

A serious issue related to implant devices is the bacterial infection and it is one of the main causes for recurrent surgery. Bacterial infection is the result of bacteria adhesion to the implant surface and biofilm formation [11]. After adhering onto the implant surface, the bacteria tend to aggregate in a hydrated polymeric matrix to form a biofilm which is the cause of many types of persistent and chronic bacterial infection [12]. It is necessary to develop biocoatings with high antibacterial activity, biosafety, and osseoconductivity. The introduction of elements Zn, Cu, Ag, La and Si made it possible to obtain the coatings with antibacterial and osteoconductive properties [13–19].

It is well established that Zn is an important trace element in human bone, and Zn species play diverse roles in biological functions, such as DNA synthesis, enzyme activity, nucleic acid metabolism, biomineralization and hormonal activity, while they also possess excellent antibacterial qualities [13–15]. Addition of Zn and Cu in biomaterials allows providing the directed antimicrobial activity to be obtained for a long time and the danger of growth of pathogenic microorganisms to be minimized [14, 15]. The antimicrobial properties of Ag^+ ions have been exploited for a long time in the biomedical fields [11, 12]. Ag^+ ions are considered to have a broad spectrum of antimicrobial properties, which is of significance for the bacterial colonization associated with biomaterial-related infections [14, 16]. La^{3+} promotes the formation of osteoclast-like cells. In addition, La^{3+} has also shown other beneficial functions, such as restraining the Ca^{2+} pump of the human red cell, treating hyperphosphataemia, resisting or preventing cancer cells from defusing [17, 18]. Si is known to be essential as a trace element in biological processes. In particular, it has been reported to have a specific metabolic role connected to bone growth [18, 19]. It is known that Si stimulates intercellular responses and plays an important role in the bone tissue formation and collagen mineralization [20].

The microarc oxidation (MAO) method allows obtaining the bioactive coatings with a porous structure and special functional properties. The MAO process is characterized by numerous microarc discharges in an electrolyte. These discharges break through a formed oxide film and cause its melting and subsequent solidification [21]. At the present time, the MAO is one of the most prospective surface treatment methods of Ti, Zr, Mg and their alloys for biomedical applications. The coating is formed during the high-temperature electrochemical processes in local microplasma regions created by microarc discharges under high voltages [9, 10, 21, 22]. During the last decade, the investigations in the field of the nanostructured biocomposites based on bioinert Ti, Zr, Nb and their alloys with a CaP coatings deposited by the MAO method have been studied in the Institute of Strength Physics and Materials Science SB RAS (ISPMS SB RAS), Tomsk [7, 21, 23].

A. Kazek-Kęsikand research group [24, 25] proposed to add the wollastonite ($CaSiO_3$) and silica (SiO_2) into the electrolyte to deposit the bioactive coatings on Ti–15Mo and Ti–13Nb–13Zr alloy by MAO method. They showed that wollastonite embedded to the coatings provides their improved biological activity. The possibility of formation of the wollastonite-calcium phosphate coatings on the Ti substrate by the MAO method was shown in our previous papers [26, 27].

This article presents the analysis of the study results of bioactive MAO coatings on Ti, Ti-Nb, Zr-Nb and Mg alloys and their promising medical application.

2. EXPERIMENT

The different types of biocomposites based on bioinert metal substrates and bioactive CaP coatings were produced by the MAO method in the various electrolytes as shown in Fig. 1. Commercially pure Ti, Ti-40Nb, Zr-1Nb and Mg-0.8Ca alloys were used as substrates. In order to carry out the MAO method the Micro-Arc-3.0 technique was used [21].
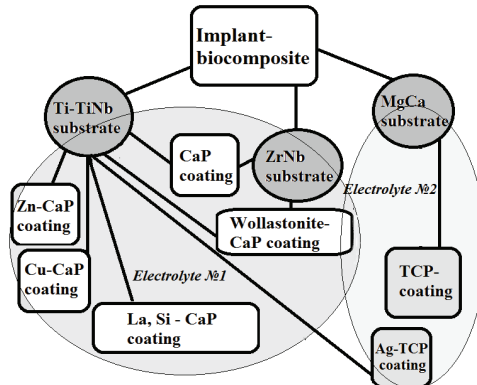
FIGURE 1. Scheme of the different types of biocomposites

The coatings were deposited in the anodic potentiostatic regime with the following parameters: pulse frequency of 50 Hz, pulse duration in the range of 100–500 μs, process duration from 5 to 10 min, pulsed voltage in the range of 130–500 V. Two types of the electrolytes were used. Electrolyte No. 1 contained the 30% aqueous solution of phosphoric acid, calcium carbonate, and Zn-, Cu- or La+Si-substituted hydroxyapatite (HA) ($Ca_{9.9}Zn_{0.1}(PO_4)_6(OH)_2$, $Ca_{9.9}Cu_{0.1}(PO_4)_6(OH)_2$ or $Ca_{9.5}La_{0.5}(PO_4)_{5.5}(SiO_4)_{0.5}(OH)_2$) [12, 18]. Electrolyte No. 1A included wollastonite ($CaSiO_3$) [15, 26, 27] and stoichiometric HA. Electrolyte No. 2 contained Na_2HPO_4, β-$Ca_3(PO_4)_2$ (β-TCP), NaOH. To deposit the Ag-incorporated coatings the $AgNO_3$ was added into the electrolyte No. 2. The morphology and structure of the coatings were examined by scanning electron microscopy (SEM, LEO EVO 50, Zeiss) in "Nanotech" center at ISPMS SB RAS and in common use center at Tomsk State University (SEM 515 Philips). The phase composition was determined by X-ray diffraction (XRD, DRON-7,"Nanotech" center) in the angular range of $2\theta = 5°–90°$ with a scan step of 0.02 with Co K_α radiation.

3. RESULTS AND DISCUSSION

Researchers indicate that the properties of MAO coatings mainly depend on the applied MAO electrical parameters, composition and concentration of electrolyte, etc. [10, 11, 21]. Figure 2a shows the typical graphs of the current density against the process duration for deposition of CaP coatings in electrolyte No. 1 under different pulsed voltages. The character of the curves with the presence of the current density steps is connected with the applied pulsed voltage to the specimen. The decrease of the current density during the MAO process is due to the growth of thick dielectric CaP coatings on metal substrates.
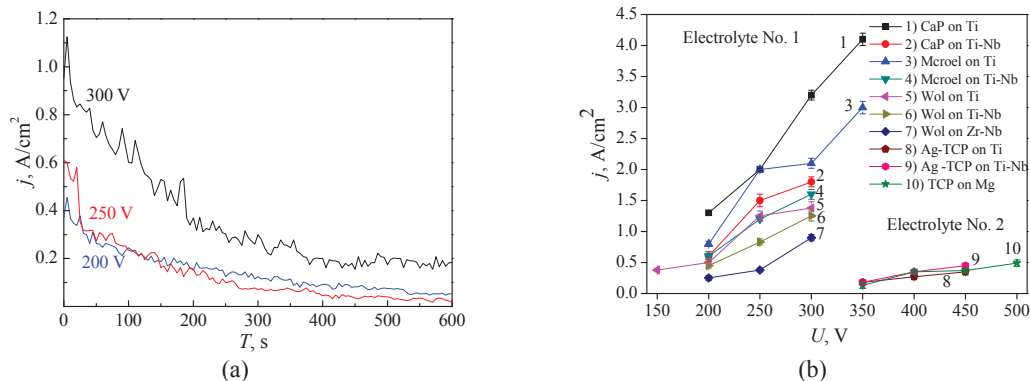

(a)

(b)

FIGURE 2. Graphs of current density against the process duration for deposition of Cu–CaP coatings (a) and graphs of initial current density against the process voltage (b)
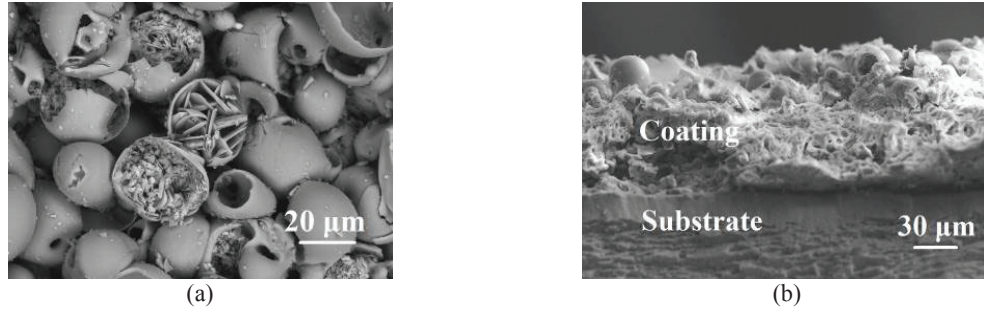
FIGURE 3. The typical SEM micrographs of the top (a) and cross-sectional (b) coatings deposited on the Ti substrate in the electrolyte No. 1

The electrolyte composition cardinally influences the MAO process of coating deposition and coating properties. In electrolytes No. 1 and 1A with acidic media (pH = 1–2) the MAO process is initiated at voltages in the range of 130–350 V (Fig. 2b). In this case, the initial current density increases from 0.25 to 4.0 A/cm^2. The maximum initial current density was 4.0 A/cm^2 for the process of CaP coatings deposition on Ti in electrolyte No. 1 with stoichiometric HA (graph 1 on the Fig. 2b). While, the MAO processes of coating deposition in electrolyte No. 1 with elements Zn, Cu, La and Si (graphs 3 and 4 on the Fig. 2b) or in electrolyte No. 1A with wollastonite (graphs 5, 6 and 7 on the Fig. 2b) are characterized by lower values of the initial current density. Also, it should be noted that the MAO process carry out at higher initial current densities on the Ti substrate than on the Ti–40Nb and Zr–1Nb alloys. It is connected with electrophysical, thermal, and thermodynamic differences between Ti and Nb, Zr metals as well as their oxides [20, 23].

The pulsed voltages in the range of 350–500 V were applied for the plasma-assisted anodic oxidation process in electrolyte No. 2 with alkaline media (pH = 10–11). But the initial current density changed from 0.13 to 0.5 A/cm^2. These values are lower than that for electrolyte No. 1. It can be explained by the differences between the composition and concentration of too electrolytes. For instance the quantity of soluble components in electrolyte No. 2 was less than that in electrolyte No. 1. Thus the more number of conductive ions which provide the electrochemical and MAO processes were in electrolyte No. 1.

3.1. Zn-, Cu- and La+Si-Incorporated Calcium Phosphate Coatings

Zn-, Cu- and La+Si-incorporated CaP coatings were formed in electrolyte No. 1 with addition of the Zn-, Cu- and La+Si-substituted HA. The thickness and average roughness (R_a) of the coatings are varied from 12 to 140 µm and from 2.5 to 8 µm, respectively. The coating morphology depends on the process voltages and the electrolyte composition. Spherical structural elements (spheres) with pores are observed on the surface of Zn–CaP, Cu–CaP and La+Si–CaP coatings (Fig. 3a). Plate-like crystals are observed in the destructed hemi-spheres on the surface of the coatings deposited under the higher MAO voltages 250–350 V. The structure of the coatings is porous (Fig. 3b).

The presence of microelements was established in the coatings. It was found that the content of Zn or Cu in the coatings is about 0.4 at % and the content of La + Si is up to 0.3 at %. The substituted elements are distributed uniformly in the coatings (Fig. 4).
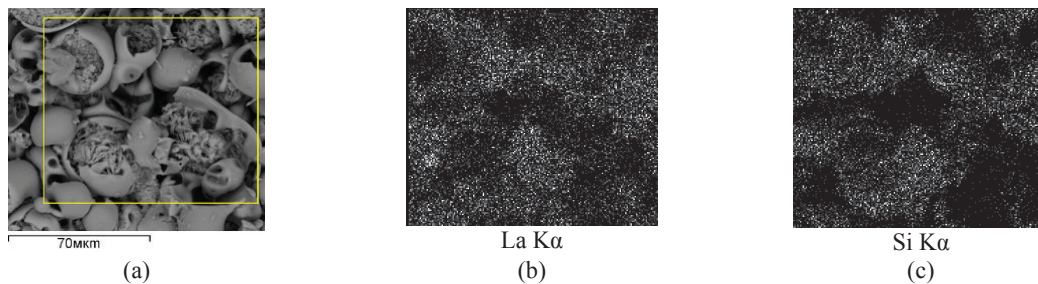

La Kα

Si Kα

(a)   (b)   (c)

FIGURE 4. SEM micrographs (a) and grey-level maps of La and Si distribution (b, c) in the La+Si–CaP coating
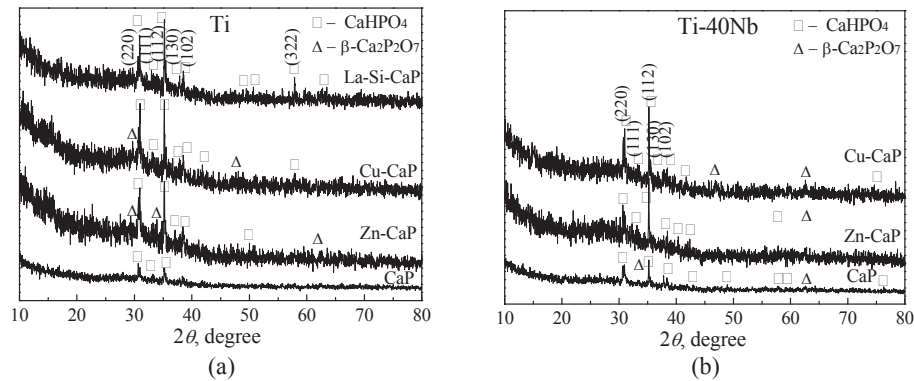
FIGURE 5. XRD patterns of the coatings formed at 300 V in theelectrolyte No. 1

The structure of the CaP, Zn–CaP, Cu–CaP and La+Si–CaP coatings deposited under the voltages 200–250 V on Ti and Ti-Nb is in the X-ray amorphous state. While reflexes of crystalline phases of monetite $CaHPO_4$ and β-calcium pyrophosphate β-$Ca_2P_2O_7$ with diffusion halos of amorphous phase are observed in XRD patterns of the coatings deposited at 300–350 V (Fig. 5). It is seen that the amount of crystalline phase in the amorphous-crystalline coatings modified with the Zn, Cu, or La+Si elements is significantly more than that in the CaP coatings without additives. We suppose, it is due to the Zn^{2+}, Cu^{2+} or La^{3+} ions participation in the electrochemical reactions during the MAO process of coating deposition.

CaP, Zn–CaP, Cu–CaP and La+Si–CaP coatings were characterized by high hydrophilic properties. The maximum contact angles with water and glycerol did not exceed 36 degrees. The adhesion strength of the coatings varied in the range of 4–16 MPa [18].

Cytotoxic tests *in vitro* of the La+Si–CaP coatings were carried out according to the MTT assay by standard ISO 10993-5-2009 [28, 29]. The mesenchymal stem cells of bone marrow washed from Wistar rat femur (Research Institute of Pharmacology and Regenerative Medicine named E.D. Goldberg, Tomsk, Russia) were used. The cell viability was evaluated using direct contact and extraction methods. The cell culture was incubated for 48 hours in a humidified atmosphere of 95% air and 5% CO_2 at 37°C. The results were analyzed using Statistics 10.0 software. The data were shown as the mean, standard derivation and standard error of the mean, as well as the median (Me), 25% quartile (Q1) and 75% quartile (Q3). To analyze the available data sets a normal distribution Kolmogorov–Smirnov test was used. Non–parametric Mann–Whitney's U–test was performed, and the differences were considered significant at $p < 0.05$. The results of biotesting by both methods showed that the proportion of surviving cells was more than 95% (Table 1). This indicates a high biocompatibility of coatings and the absence of a cytotoxic effect on cells.

Zn–CaP and Cu–CaP coatings showed a clear antimicrobial effect against *S. aureus* strain 209 through the products of its dissolution due to the release of the ions Zn^{2+} or Cu^{2+}. Zn–CaP coatings demonstrated the more noticeable antibacterial effect on microorganisms. At the same time, a significant toxic effect of such coatings on rat bone marrow cells was observed. It may be due to the indiscriminate action of Zn^{2+} ions with respect to the induction of death of eukaryotic and prokaryotes cells.

TABLE 1. Cell viability (percentage) of mesenchymal stem cells cultivated for 48 hours in direct contact with coatings and in their extracts, Me(Q$_1$ – Q$_3$)

Groups, n = 6	The number of viable cells, %	
	Direct contact method	Extract method
Cell culture without coating, control group	100	100
Cell culture with coating	95.8 (90.2–100.0) ($p < 0.05$)	97.9 (89.2–100.0) ($p < 0.05$)

<div align="center">Si Kα</div>

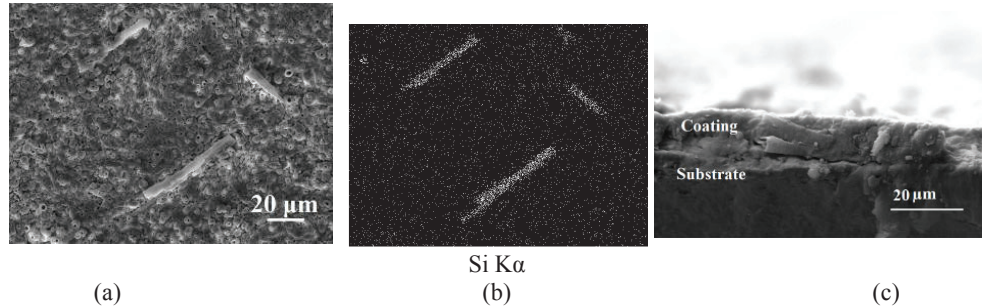<div align="center">(a)   (b)   (c)</div>

FIGURE 6. SEM micrographs (a, c) and grey-level maps (b) for the wollastonite–CaPcoatings produced at 150 V

3.2. Wollastonite-Incorporated Calcium Phosphate Coatings

Wollastonite (50.0–53.0 SiO_2, 45.0–48.0 CaO, 0.4–1.0 MgO, 0.1–0.3 Al_2O_3, 0.05–0.2 Fe_2O_3, wt %) was added into the electrolyte No. 1A. It was supposed that the wollastonite crystals embedded into the coating structure can increase the mechanical characteristics of the coatings and enhance the biological activity [20, 24, 25]. Elongate wollastonite particles with sizes in the range of 40–100 μm were observed in SEM images of the coatings formed at the MAO voltage of 150V (Figs. 6a, 6c). Large amount of Si was localized in the areas with needle-like particles in the coatings (the areas are marked by white color in Fig. 6b).

The XRD patterns show the presence of crystalline phases $CaSiO_3$ and Ti (Fig. 7a). Diffusion halo of amorphous phase is also observed in the XRD patterns. The increase in the pulse duration from 100 to 500 μs at the low voltage of 150 V leads to the formation of wollastonite-incorporated calcium phosphate (W–CaP) coating with adhesion strength up to 57 MPa (Fig. 7b). We suppose that the embedding of many wollastonite crystals into the coatings provides an increase in mechanical characteristics as a result of the formation of a reinforcing structure.

The increase in the MAO voltage from 200 to 300 V leads to dissociate of the wollastonite (Fig. 8a). It can be a result of high temperatures in the micro–discharge areas promoted the dissociation of wollastonite crystals during the MAO process. In this case, the Si is distributed homogeneously throughout the coating (Fig. 8b). Diffusion halo is observed in selected area diffraction (SAD) pattern that indicate the amorphous microstructure of the coatings (Fig. 8c). The biological studies using osteoblast-like cells were carried out by the authors [25] and showed that the wollastonite in the oxide layers formed on the Ti–13Nb–13Zr alloy surface by the MAO process promotes the cell adhesion and proliferation.

The cytotoxic test of W–CaP coatings was performed according to ISO 10993-5 with 0.4% trypan blue. Prenatal stromal stem cells prepared from a human lung (Stem Cells Bank Ltd., Tomsk, Russia) were used. The percentage of viable (unstained by trypan blue) cells in cases of W–CaP coating on Ti ($94.0 \pm 1.5\%$), Ti–40Nb ($94.5 \pm 0.8\%$) or Zr–Nb ($93.0 \pm 1.2\%$) did not differ statistically from that for the background ($96.4 \pm 0.5\%$) after 1 h co-culturing.

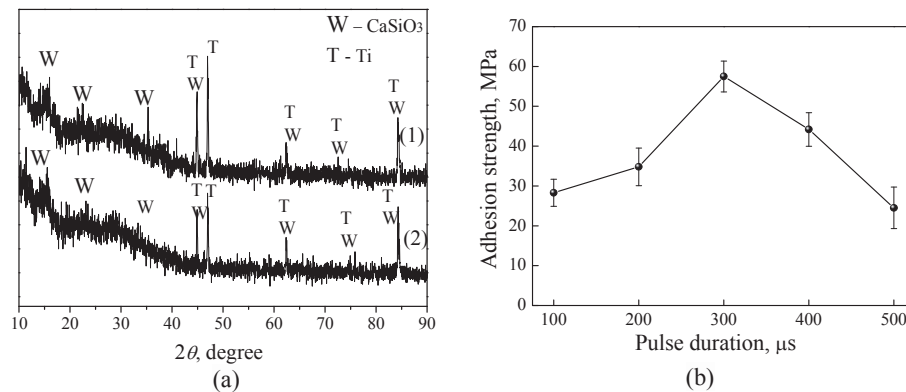<div align="center">(a)   (b)</div>

FIGURE 7. XRD patterns (a) for various process and pulse durations: (1) 5 min, 300 μs; (2) 10 min, 100 μs; graph of the adhesion strength (b) against the pulse duration for the W–CaP coatings produced at 150 V
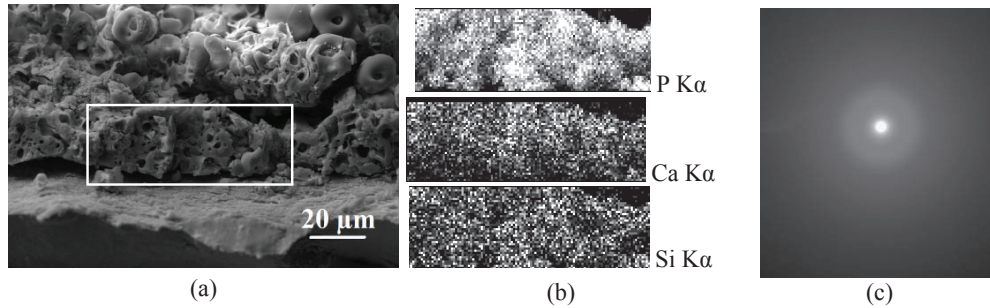
FIGURE 8. SEM micrographs (a), grey-level maps (b) and SAD pattern (c) of W–CaP coating produced at 200 V

The stromal cell culture secretes enzyme alkaline phosphatase (ALP) into extracellular fluid. Thereby the osteogenic potential of fibroblast-like adherent cells is revealed (Table 2). ALP is a marker of functional activity (osteogenic differentiation and maturation) of stromal stem cells [30].

It is also known that a variation in the potassium and sodium content in extracellular fluid indicates about violate of the physiological mechanisms of cell membrane permeability. In these studies the concentration of potassium ions in the extracellular fluid is unchanged and the concentration of sodium ions is slightly changed as the cell culture interacts with the W–CaP coating (Table 2). Thus, the W–CaP coatings do not exert toxic effect on the morphofunctional status of the studied cells.

3.3. Ag-Incorporated Calcium Phosphate Coatings

The Ag-incorporated CaP coatings were formed on Ti and Ti-Nb substrates in electrolyte No. 2 with alkaline media. The structure of the coatings is homogeneous with pores and isometric particles (Fig. 9a). It is revealed that the size and shape of these particles are identical to that of β-TCP particles shown in the Fig. 9b. The elemental composition of the particles in the coatings is mainly presented by O, P and Ca elements with Ca/P ratio ~ 1. It may be assumed that with the current density decreasing due to the growth of dielectric CaP coatings (Fig. 2a) the intensity of micro-discharges decrease. It triggers to the transport of the β-TCP particles from the electrolyte to the coating surface.

The phase composition of coatings was presented by β-TCP, α-TCP, HA and TiO_2 in the rutile and anatase modifications (Figs. 9c, 9d). It was found that the crystalline phase of TCP is formed in the coatings on Ti at high voltages 400–450 V. While, the coatings on Ti-Nb alloy deposited at lower voltage 350 V contain crystalline CaP phases. With increasing of the MAO voltage from 400 to 450 V the X-ray amorphous structure is formed (Fig. 9d).

TABLE 2. Results of ion concentration and an activity of alkaline phosphatase measurement in intercellular fluids of prenatal human stromal cells (FL-42) in 7 days of the contact with tested specimens of microarc coatings on various metal substrates, Me (Q1-Q3)

Groups, $n = 3$	Potassium, mM	Sodium, mM	Activity of alkaline phosphatase, U/L
Culture medium without cells, group 0 (background)	7.9 (7.8–7.9)	138.5 (138.0–140.0)	388.0 (380.0–389.0)
Stromal cells without specimens, group 1 (control)	7.8 (7.8–7.9)	141.5 (141.0–143.0) P0<0.05	400.5 (400.0–403.0) P0 < 0.001
W–CaP coating on Ti, group 2	7.5 (7.5–7.8)	139.0 (137.0–142.0)	395.0 (376.0–412.0)
W–CaP coating on Ti40Nb, group 3	7.7 (7.7–7.9)	140.0 (140.0–143.0)	416.0 (405.0–417.0) P1 < 0.05

Note: P0, P1—statistically significant differences with values of corresponding groups in accordance with Mann–Whitney's U-test; *n*—the number of tested specimens (probes).
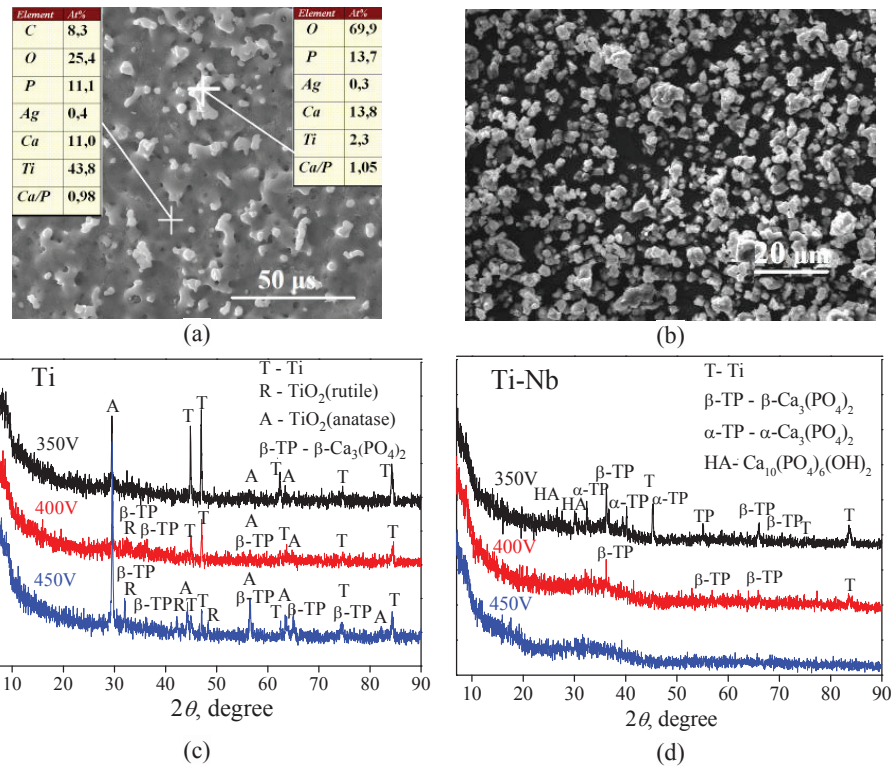
FIGURE 9. SEM micrographs of the Ag-incorporated coating deposited on Ti at 450 V(a) and of the β-TCP powder (b); XRD patterns of the coatings formed on Ti (c) and Ti–40Nb (d) under the different MAO voltages

With increasing in the pulsed voltage from 350 to 450 V the silver content and Ca/P ratio in the coatings increase from 0.1 to 0.4 at % and from 0.2 to 1.1, respectively. The silver distribution in the coatings is uniform. It is known that the rather small concentration of silver up to 3.5 at % can provide a significant antibacterial effect [12].

The maximum values of the thickness and roughness (R_a) equaled to 37 µm and 3.5 µm, respectively, were obtained for the Ag-incorporated on the Ti substrate. The coatings on Ti–Nb alloy had higher values of the thickness and roughness (R_a) equaled to 70 µm and 6.5 µm, respectively for the all values of voltage.

With increasing in the thickness and roughness of the coatings their wettability increases. High free surface energy values of 76–110 mN/m indicate the good hydrophilic properties of Ag-containing coatings on both substrates. The contact angles decreased linearly to 10 degrees with water and to 35 degrees with glycerol with increasing of the process voltage. It is associated with the surface roughness growth as well as with the increase in the coating surface area.

3.4. Coatings on Mg-0.8Ca Alloy

The SEM results indicate that the MAO coatings deposited on Mg-0.8Ca alloy under the voltages of 350–500 V in alkaline electrolyte No. 2 have porous morphology and structure (Figs. 10a, 10b). Pore sizes were in the range of 2.0–5.0 µm. The authors reported [31] that with increasing in the applied voltage a large number of irregular shaped pores were formed in the MAO coatings. The β-TCP particles are observed only on the coating surface and absent in the coating structure (Fig. 10b).

The increase in the MAO voltage to 500 V and process duration to 10 min leads to the linear increase in the coating thickness and roughness (R_a) to 140 µm and 8 µm, respectively. The coating phase composition is represented by the following crystalline compounds β-TCP, MgO-periclase and HA (Fig. 10c). Reflexes corresponding to Mg substrate are observed in XRD patterns of the coatings deposited under the voltage of 350–450 V. Also, the diffusion halo from amorphous phase of calcium phosphate substance is observed in XRD patterns of the coatings in the angles range of 10–45 degrees.
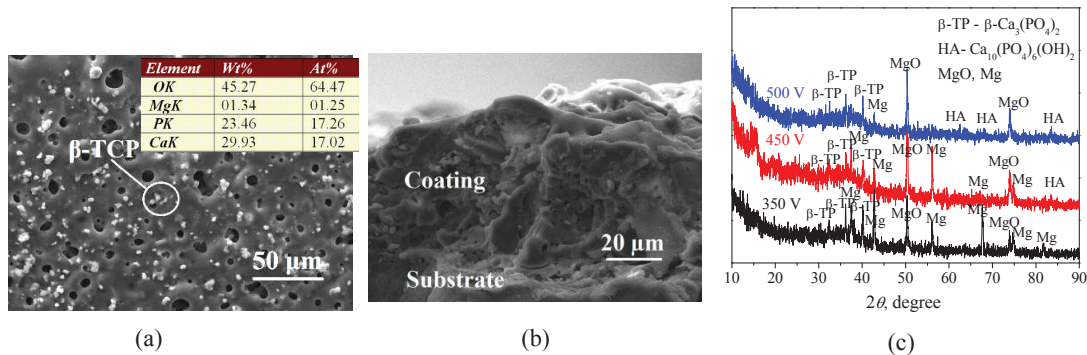
Element	Wt%	At%
OK	45.27	64.47
MgK	01.34	01.25
PK	23.46	17.26
CaK	29.93	17.02

β-TCP

Coating

Substrate

50 µm

20 µm

β-TP - β-Ca$_3$(PO$_4$)$_2$
HA- Ca$_{10}$(PO$_4$)$_6$(OH)$_2$
MgO, Mg

(a)   (b)   (c)

FIGURE 10. SEM micrographs of the top-view (a) and cross-section (b) of the coating deposited on Mg-0.8Ca at 450 V; XRD patterns (c) of the coatings formed under different voltages

The investigations of the corrosion resistance of the Mg-0.8Ca alloy without coating and the CaP coatings on Mg-0.8Ca alloy were carried out using 3.5% NaCl solution (Fig. 11). The defects on the Mg-0.8Ca alloy surface started to form during the first day of soaking in the NaCl solution (Fig. 11b). After 3.5 days soaking the gel-like compounds were observed on the alloy surface as a result of the alloy dissolution (Fig. 11c).

The coatings on Mg-0.8Ca alloy showed a higher corrosion resistance than Mg-0.8Ca alloy without coating (Figs. 11d–11f). When the coatings were aged in the NaCl solution the destruction of them was observed after 3.5 days (Figs. 11e, 11f). Moreover, this process occurred more intensively on the surface of thing coatings deposited under the lower voltage of 350 V (Fig. 11f).

The graphs of the weight loss against soaking time show the higher rate of weight loss for uncoated Mg-0.8Ca alloy than for the CaP coatings (Fig. 12). There is evidence that the coatings are protective reducing the corrosion rate of the alloy. Also, the CaP compounds in the coatings are favorable for osseointegration initiating the new boneformation [1].

4. CONCLUSIONS

Electrolyte composition and the MAO process parameters substantially effect on the coating structure and properties. The coatings with a high thickness and roughness (R_a) up to 140 and 3.5 µm, respectively, were formed in the acid electrolyte–suspension. The coating surface morphology was represented by spheroidal structural elements. The Zn–, Cu–, La–Si–CaP coatings produced at 200–250 V had mainly X-ray amorphous structure.

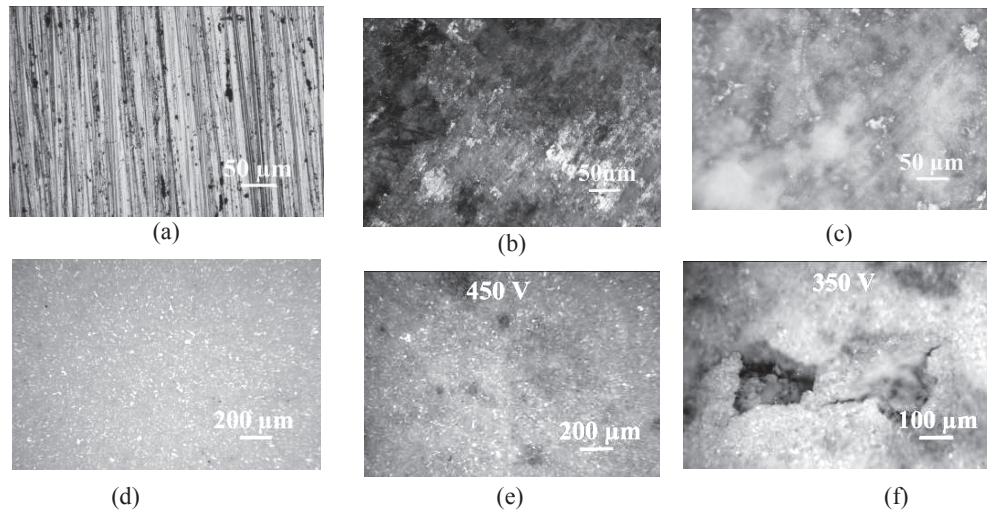(a)   (b)   (c)

(d)   (e)   (f)

FIGURE 11. Optical images of the Mg-0.8Ca alloy (a–c) and the coatings on Mg-0.8Ca alloy (d–f) before the soaking in 3.5% NaCl solution (a, d) and after the soaking for 15 h (b) and 85 h (c, e, f)
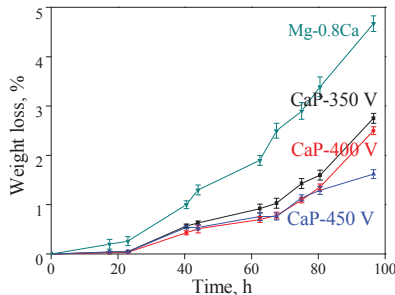
FIGURE 12. Graphs of the weight loss against the time of dissolution

Increase of the voltage to 300–350 V led to the formation of crystalline phases of monetite $CaHPO_4$ and β-calcium pyrophosphate β-$Ca_2P_2O_7$ in the coatings. The coatings had high hydrophilic properties. The maximum contact angles with water and glycerol did not exceed 36 degrees. The content of Zn, Cu or La and Si elements in the coatings was about 0.4 at %. The Ca/P ratio was up to 0.7. Due to the amorphous-crystalline structure with presence of $CaHPO_4$ and β-$Ca_2P_2O_7$ the coatings have a high rate of dissolution that can provide the controlled releaserate of antibacterial elements.

The wollastonite-CaP coatings were produced at 150 V. The embedding of wollastonite crystals in the coatings led to the increase in adhesion strength up to 57 MPa as the result of the formation of a reinforcing structure. The increase in the voltage from 200 to 300 V led to dissociate of the wollastonite due to the high temperatures in the micro–discharge areas.

The Ag-containing coatings with a homogeneous porous structure were formed in the alkaline electrolyte. The coating thickness and roughness (R_a) were less than those for the coatings formed in the acid electrolyte–suspension. With increasing in the MAO voltage the silver content and Ca/P ratio increased to 0.4 at % and 1.1, respectively. The coating phase composition was represented by TiO_2 (rutile and anatase), β-TCP and α-TCP.

The presence of crystalline phases, β-TCP, MgO—periclase, $Ca_{10}(PO_4)_6(OH)_2$—hydroxyapatite was revealed in the coatings on Mg-0.8Ca alloy deposited in the alkaline electrolyte. These crystalline phases can prevent rapid resorbtion of the Mg alloy and improve the biological compatibility of the implants.

The absence of cytotoxic action, high viability of stromal stem cells and antibacterial effect of the coatings allow recommending the biocomposite materials with MAO coatings for the medical applications. Wollastonite-incorporated biocoatings have high adhesion strength with the base material and increase the strength of fixing implants to bone tissue. Microelements-incorporated coatings with controlled rate of bioresorption and high ability to osseointegration with bone tissue are important for submerged osteosynthesis.

The biocomposites based on Ti-Nb alloys with good biomechanical properties are promising for the traumatology and orthopedics. Zr and its alloys are perspective for the dentistry and load-bearing prostheses due to the high strength and corrosion resistance. The implants from the resorbed magnesium alloys with a controlled rate of bioresorption and good biomechanical properties are of interest if it is necessary to exclude the reoperation.

ACKNOWLEDGMENTS

REFERENCES

1. X. Li, C. Chu, and P. K. Chu, Bioactive Mat. **1**, 77–84 (2016).
2. C. Y. Zhang, R. C. Zeng, C. L. Liu, and J. C. Gao, Surf. Coat. Tech. **204**, 3636–3640 (2010).
3. K. Zhuravleva, R. Muller, L. Schultz, J. Eckert, A. Gebert, M. Bobeth, and G. Cuniberti, Mat. Design. **64**, 1–8 (2014).

4. K. Zhuravleva, M. Bönisch, S. Scudino, M. Calin, L. Schultz, J. Eckert, and A. Gebert, Powder Tech. **253**, 166–171 (2014).

5. Y. P. Sharkeev, A. Y. Eroshenko, Z. G. Kovalevskaya, A. A. Saprykin, E. A. Ibragimov, I. A. Glukhov, M. A. Khimich, P. V. Uvarkin, and E. V. Babakova, Russ. Phys. J. **59**, 430–434 (2016).

6. J. Y. Ha, Y. Tsutsumi, H. Doi, N. Nomura, K. H. Kim, and T. Hanawa, Surf. Coat. Tech. **205**, 4948–4955 (2011).

7. E. V. Legostaeva, K. S. Kulyashova, E. G. Komarova, M. Epple, Yu. P. Sharkeev, and I. A. Khlusov, Mat.-wiss. u. Werkstofftech. **44**, 188–197 (2013).

8. Z. Zou, W. Xue, X. Jia, J. Du, R. Wang, and L. Weng, Surf. Coat. Tech. **222**, 62–67 (2013).

9. G. Y. Liu, J. Hu, Z. K. Ding, and C. Wang, Mat. Chem. Phys. **130**, 1118–1124 (2011).

10. T. S. N. S. Narayanan, I. S. Park, and M. H. Lee, Prog. Mat. Sci. **60**, 1–71 (2014).

11. G. A. Fielding, M. Roy, A. Bandyopadhyay, and S. Bose, Acta Biomat. **8**, 3144–3152 (2012).

12. V. Kotharu, R. Nagumothu, C. B. Arumugam, M. Veerappan, Su. Sankaran, M. A. Davoodbasha, and T. Nooruddin, Ceramics Int. **38**, 731–740 (2012).

13. H. Hu, W. Zhang, Y. Qiao, X. Jiang, X. Liu, and C. Ding, Acta Biomat. **8**, 904–915 (2012).

14. N. Matsumoto, K. Sato, K. Yoshida, K. Hashimoto, and Y. Toda, Acta Biomat. **5**, 3157–3164 (2009).

15. M. B. Sedelnikova, E. G. Komarova, and Yu. P. Sharkeev, J. Key Eng. Mat. **695**, 144–151 (2016).

16. A. Ewald, D. Hösel, S. Patel, L. M. Grover, J. E. Barralet, and U. Gbureck, Acta Biomat. **7**, 4064–4070 (2011).

17. D. G. Guo, A. H. Wang, Y. Han, and K. W. Xu, Acta Biomat. **5**, 3512–3523 (2009).

18. E. G. Komarova, M. V. Chaikina, M. B. Sedelnikova, and Y. P. Sharkeev, AIP Conf. Proc. **1760**, 020031 (2016).

19. M. Palard, E. Champion, and S. Foucaud, J. Solid State Chem. **181**, 1950–1960 (2008).

20. M. B. Sedelnikova, Y. P. Sharkeev, E. G. Komarova, I. A. Khlusov, and V. V. Chebodaeva, Surf. Coat. Tech. **307**, 1274–1283 (2016).

21. Y. P. Sharkeev, S. G. Psakhie, E. V. Legostaeva, A. G. Knyazeva, A. Y. Smolin, et al, *Biocomposites Based on Calcium-Phosphate Coatings, Nanostructured and Ultrafine-Grained Bioinert Metals, Their Biocompatibility and Biodegradation* (Publishing House of Tomsk State University, Tomsk, 2014), 596 p.

22. S. Liu, B. Li, C. Liang, H. Wang, and Z. Qiao, Appl. Surf. Sci. **362**, 109–114 (2016).

23. E.V. Legostaeva, Y. P. Sharkeev, M. Epple, and O. Prymak, Russ. Phys. J. **56**, 1130–1136 (2014).

24. A. Kazek-Kęsik, G. Dercz, K. Suchanek, I. Kalemba-Rec, J. Piotrowski, and W. Simka, Surf. Coat. Tech. **276**, 59–69 (2015).

25. A. Kazek-Kęsik, M. Krok-Borkowicz, A. Jakóbik-Kolon, E. Pamuła, and W. Simka, Surf. Coat. Tech. **276**, 23–30 (2015).

26. M. B. Sedelnikova, E. G. Komarova, Y. P. Sharkeev, and T. V. Tolkacheva, AIP Conf. Proc. **1683**, 020202 (2015).

27. Y. P. Sharkeev, M. B. Sedelnikova, E. G. Komarova, and I. A. Khlusov, AIP Conf. Proc. **1688**, 060002 (2015).

28. J. P. Mather and P. E. Roberts, *Theory and Technique* (Plenum Press, New York, 2002).

29. S. Giri, K. Nieber, A. Acikgo, S. Pavlica, M. Keller, and A. Bader, Mol. Cell. Biochem. **336**, 137–149 (2010).

30. I. A. Khlusov, N. M. Shevtsova, and M. Y. Khlusova, Meth. Mol. Biol. **1035**, 103–119(2013).

31. Y. Gu, W. Xiong, C. Ning, and J. Zhang, J. Mater. Eng. Perform **21**, 1085–1090 (2012).